Flexural behaviour of 7A04-T6 high-strength aluminium alloy SHS and RHS beams under moment gradient

Li, Beibei; Wang, Yuanqing ; Zhang, Ying; Yuan, Huanxin; Zhi, Xinhang; Baniotopoulos, Charalampos

DOI:
10.1016/j.engstruct.2022.114138

Flexural behaviour of 7A04-T6 high-strength aluminium alloy SHS and RHS beams under moment gradient

Beibei Li[a], Yuanqing Wang[a,b], Ying Zhang[a,*] (corresponding author), Huanxin Yuan[c], Xinhang Zhi[a], Charalampos C.Baniotopoulos[d]

[a] *Department of Civil Engineering, Tsinghua University, Beijing 10084, PR China*

[b] *Key Laboratory of Civil Engineering Safety and Durability of China Ministry of Education, Tsinghua University, Beijing 100084, PR China;*

[c] *School of Civil Engineering, Wuhan University, Wuhan 430072, PR China*

[d] *School of Engineering, University of Birmingham, Edgbaston, Birmingham, B15 2TT, UK*

ABSTRACT: High-strength aluminium alloys would further reduce the cross-section dimensions, and consequently avoid inaccessible extrusion process for great cross-section members and accelerate the construction speed in comparison with normal-strength aluminium alloys. 16 tests on extruded square and rectangular hollow sections (SHS/RHS) subjected to three-point bending were carried out in this paper, with width-to-thickness ratios ranging from 6.07 to 18.22. The material properties, failure modes, moment resistance, end rotation capacity and strain response of specimens were fully reported. Finite element (FE) models were developed and validated against the experimental results. Upon validation, an extensive parametric study over a wide range of cross-sectional slenderness and width-to-height ratios was performed. The experimental and numerical results were used to evaluate the applicability of the current design provisions in Chinese, European and American codes, as well as the proposed continuous strength method (CSM) extended to the 7A04-T6 high-strength aluminium alloy, which is not included in the codes. The results showed that the predictions yielded by the three standard design methods were relatively conservative, while significantly improved resistance predictions were obtained through application of the revised CSM-based approach. The four design methods were safely feasible to the design of 7A04-T6 high-strength aluminium alloy SHS and RHS beams according to the reliability analysis.

KEYWORDS

High-strength aluminium alloy; Square and rectangular hollow sections; Three-point bending; Finite element analysis; Experiments; Continuous strength method (CSM)

1. Introduction

Aluminium alloy is an attractive material with advantages of high strength-to-weight ratio, favourable corrosion resistance, fast fabrication, low maintenance cost, flexibility in cross-section forms [1]. Consequently, it is not surprising that the application of aluminium alloys is growing rapidly in structural engineering, such as space structures, bridges and prefabricated frameworks. Several existing structural design standards, including the Chinese code for design of aluminium structures (GB 50429-2007) [2], European standard for design of aluminium structures (EC9-2007) [3] and American aluminium design manual (AA-2015) [4], provide rules for ordinary aluminium alloys, and 6xxx-series aluminium alloys with a nominal yield strength ($f_{0.2}$) of around 300 MPa are currently the most widely used in buildings and constructions. However, on the one hand, great cross-section members are generally required due to the relatively low strength of 6xxx-series aluminium alloys, on the other hand, the member cross-section dimensions are strictly limited by the capacity of the extrusion equipment. The existing maximum height of extruded 6061-T6 aluminium alloy box-section beams is 550 mm and is used in Usnisa Palace on the Niushou Mountain in Nanjing, China [5]. With the development of structural engineering toward a large-span, complex and heavy loading environment, and the urgent demands for rapidly assembled temporary structures in case of suddenly happened natural disasters or public health events, new requirements are put forward on the high-performance of aluminium alloy materials. 7xxx-series aluminium alloys, such as the 7A04-T6 and 7075-T6, generally have high yield strengths up to about 500 MPa, which are substantially greater than those of 6xxx-series ordinary aluminium alloys. The higher ultimate strengths of 7xxx-series aluminium alloys would further reduce

the cross-section dimensions, and consequently lighten the weight of structural members, accelerate the construction speed and avoid inaccessible extrusion process for super large cross-section members. The next version GB 50429 [2] will be covering relevant provisions of 7A04-T6 and 7075-T6 high-strength aluminium alloys to promote the application of 7xxx-series high-strength aluminium alloys in structural engineering.

Most of the studies about constructional 7xxx-series high-strength aluminium alloys focus on their material properties. Zhang et al. [6] conducted dynamic tensile tests on 7075-T6 high-strength aluminium alloy at various strain rates. Wang et al. [7] investigated the constitutive relationship of 7A04-T6 high-strength aluminium alloy by static cyclic loading tests. Chen et al. [8] carried out post-fire static tensile tests on 7075-T73 high-strength aluminium alloy subjected to various temperatures and cooling methods. Karolczuk et al. [9] experimentally and theoretically studied the fatigue failure probabilities of 7075-T651 high-strength aluminium alloy. Limited studies on 7xxx-series high-strength aluminium alloy members have been reported to date. Wang et al. [10, 11] carried out a series of tests on 7A04-T6 high-strength aluminium alloy pin-ended and fixed-ended angle-section columns under axial compression, with numerical studies to assess the accuracy of current design approaches. Rong at al. [12] tested 39 7A04-T6 high-strength aluminium alloy tubular columns under axial compression.

With regard to the aluminium alloy beam, which is deemed as one of the basic loading members (e.g. axial compression, eccentric compression and bending), most researchers [13-28] focused on the bearing and deformation capacities of flexural members made of 6061-T6, 6063-T5 and 6082-T6 ordinary aluminium alloys, such as Moen et al. [13], Zhu and Young [14], Kim and Peköz [15], Su et al. [16-19], Feng et al. [20, 21], Nastri et al. [22-26], Zhao and Zhai [27], Bock et al. [28]. However, few studies on bending behaviours of 7A04-T6 high-strength aluminium alloy SHS and RHS beams

subjected to moment gradient loading have been reported, which gives rise to a great restriction on the application and development of high-strength aluminium alloys in structural engineering.

The purpose of this investigation is to promote the application of the high-strength aluminium alloy in structural engineering, considering the higher demand for the members' load-carrying capacities in engineering applications and the limitation of aluminium alloy extrusion equipment for large sections. Therefore, an experimental and numerical investigation of 7A04-T6 high-strength aluminium alloy SHS and RHS beams is presented in this paper. First, 16 specimens with various extruded cross-section slenderness were tested under three-point bending. The failure modes, mid-span moment-end rotation curves and the ultimate resistance of the beams were then analysed. Based on the developed and validated finite element (FE) models, numerical parametric studies were conducted. The continuous strength method (CSM) extended to the 7A04-T6 high-strength aluminium alloy was proposed for flexural behaviour of the beams. Furthermore, the numerical and experimental results were employed to assess the accuracy of design rules of the Chinese, European and American standards, as well as the proposed CSM. Finally, the reliability analysis was conducted to evaluate the applicability of the four design methods.

2. Experimental programme

2.1 Test specimens

In order to evaluate the flexural resistance, rotation capacity and strain hardening performance of the high-strength aluminium alloy beams, a total of 16 specimens of square and rectangular hollow sections (SHS/RHS) were tested under three-point bending. All specimens were the extruded 7A04-T6 high-strength aluminium alloy SHS/RHS members with rounded corners. Details of specimens are listed in Table 1, using the symbols shown in Fig. 1, where L_e is the simply supported length. All specimens were labelled by their cross-section type, test configuration and cross-section dimensions.

Fig. 1 Schematic diagram of cross-section

Table 1 Measured dimensions of specimens

Specimen	B (mm)	H (mm)	t (mm)	L_e (mm)	b_f/t	h_w/t	v_o (mm)	Section type under bending
STB80-A	80.10	80.03	4.98	800	14.08	14.07	0.314	Class 3
STB80-B	79.88	79.90	4.64	800	15.21	15.21	0.427	Class 4
STB120-A	120.38	120.39	10.23	1200	9.76	9.77	0.605	Class 2
STB120-B	120.46	120.45	10.21	1200	9.80	9.80	0.391	Class 2
RTB100-50-W-A	100.20	49.48	6.03	1200	14.62	6.21	0.482	Class 3
RTB100-50-W-B	100.15	49.53	6.14	1200	14.32	6.07	0.704	Class 3
RTB100-50-S-A	49.35	99.83	5.95	1200	6.29	14.78	0.319	Class 1
RTB100-50-S-B	49.40	99.92	5.96	1200	6.29	14.76	0.428	Class 1
RTB100-70-W-A	100.38	70.42	8.46	1200	9.87	6.33	0.318	Class 2
RTB100-70-W-B	100.46	70.20	8.49	1200	9.83	6.27	0.635	Class 2
RTB100-70-S-A	70.39	100.40	8.49	1200	6.29	9.83	0.501	Class 1
RTB100-70-S-B	70.40	100.42	8.52	1200	6.26	9.78	0.415	Class 1
RTB60-30-W-A	60.10	30.05	2.97	800	18.22	8.11	0.671	Class 4
RTB60-30-W-B	60.06	30.15	3.00	800	18.04	8.06	0.550	Class 4
RTB60-30-S-A	29.99	60.04	3.01	800	7.96	17.93	0.715	Class 2
RTB60-30-S-B	30.40	60.30	3.08	800	7.86	17.56	0.513	Class 2

Taking the label “RTB100-50-W-A” as an example, it represents the RHS (R) specimen under three-point bending (TB), with nominal cross-section dimensions of 100-mm width and 50-mm height. The symbol “W” denotes the specimen was loaded about the weak axis of the cross-section, while the specimen RTB100-50-S-A was loaded about the strong axis. The last letter “A” or “B” refers to the repeated specimens A and B with the same dimensions. As shown in Table 1, the width-to-thickness ratios for the flange (b_f/t) and the height-to-thickness ratios for the web (h_w/t) were respectively ranged from 6.26 to 18.22 and 6.07 to 17.93, which consequently covered four classes of cross-sections according to EC9-2007 [3], making the experimental research wide-ranging in engineering practice. Prior to testing, the initial overall geometric imperfections (v_o) were measured using a theodolite and a vernier caliper [29], and taken from the maximum values along the specimen length, all of which were

less than $L/1000$.

2.2 Material properties

The stress-strain properties of the 7A04-T6 high-strength aluminium alloy used to manufacture specimens were obtained by tensile coupon tests. The tensile coupons were extracted along the longitudinal direction of specimens and three repeated coupon tests were conducted [30]. All the tensile coupon tests were performed using a 1000-kN hydraulic testing machine, with two strain gauges and one extensometer recording the strain response during testing. Fig. 2 shows the schematic diagram and failure mode of brittle fracture with no obvious necking of tensile coupons. Some specimens with cracks were relatively close to the clamping heads, while they were almost within the gauge length, and were also reported in References [11, 29]. The measured stress-strain curves of coupons are presented in Fig. 3. Two coupons with nominal thickness of 6 mm showed a little serration after reaching $f_{0.2}$, which probably due to a not well clamping. This phenomenon was also observed in References [10-12, 14]. The key measured average material properties are given in Table 2, in which E is the Young's modulus; $f_{0.1}$ and $f_{0.2}$ are the 0.1% and 0.2% proof (equivalent yield) stresses, respectively; f_u and ε_u are the ultimate stress and corresponding strain; n is the exponent of the Ramberg-Osgood expression [31], which is given by $\varepsilon = \sigma/E+0.002(\sigma/f_{0.2})^n$ and $n = \ln(0.002/\varepsilon_{o,u})/\ln(f_{0.2}/f_u)$, where $\varepsilon_{o,u} = \varepsilon_u-0.002$.

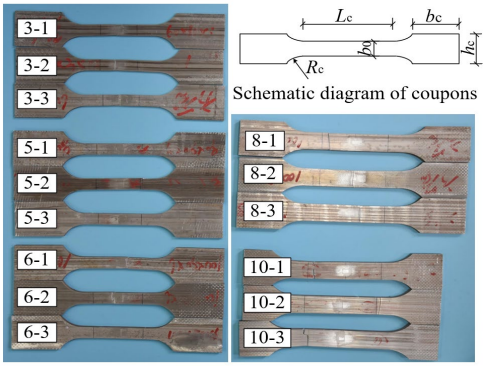

Fig. 2 Schematic diagram and fracture of coupons

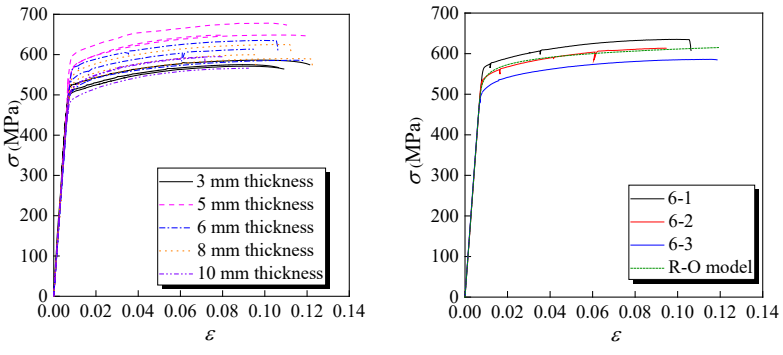

Fig. 3 Stress-strain curves of aluminium alloy tensile coupons

2.3 Test setup and instrument configurations

All simply supported specimens were monotonically loaded by a 2000-kN servo-controlled hydraulic

actuator under the three-point bending, as illustrated in Fig. 4. The free and fixed steel rollers, together with stiffening clamping plates with the width of 250 mm, were employed at specimen ends for simply

Table 2 Summary of material properties

Section ($B\times H\times t$, mm)	b_0 (mm)	t (mm)	L_c (mm)	R_c (mm)	b_c (mm)	h_c (mm)	E (GPa)	$f_{0.1}$ (MPa)	$f_{0.2}$ (MPa)	f_u (MPa)	ε_u (%)	n
60×30×3	15	3	80	30	45	60	73.64	510.37	514.49	577.53	9.22	32.99
100×50×6	15	5	80	30	45	60	75.43	571.53	581.03	658.32	9.41	30.60
80×80×6	15	6	80	30	45	60	71.27	534.83	540.93	611.57	10.16	31.93
100×70×8	25	8	120	40	50	60	74.70	512.37	530.83	604.72	10.47	30.18
120×120×10	25	10	120	40	50	40	73.70	498.43	507.47	584.77	8.00	25.78
Mean		-					73.75	525.51	534.95	607.38	9.45	30.30
COV		-					0.022	0.058	0.057	0.052	0.131	0.095

support conditions. The bearing plates with the width of 100 mm were also arranged at end supports and mid-span loading point to avoid load concentration. Two ±25 mm linear variable differential transformers (LVDTs) and one ±100 mm LVDT were respectively positioned at end supports and mid-span loading point to measure the end rotation and mid-span vertical deflection, as illustrated in Figs. 4 and 5. Additionally, a total of 18 strain gauges were attached on the flanges and webs for each specimen at the $L_e/4$ position and 65 mm away from the mid-span loading point. The load, displacement and strain were recorded in real time at 0.5 s intervals using DH3816N Static Strain acquisition System made by Jiangsu Donghua Analytical Instrument Co., Ltd.

(a) Loading setup (b) The end clamping device

Fig. 4 Experimental setup

A preliminary load of $0.05P_u$ ($P_u=4W_{pl}f_{0.2}/L_e$, where W_{pl} is the plastic section modulus) was applied on the specimen prior to the formal loading test to check and calibrate the effectiveness of the experimental configurations and data-acquisition system. The loading rates were $0.02P_u$/min before

reaching 0.8P_u, after which the loading process was controlled by displacement at a rate of 0.8 mm/min [16, 17] till the load no longer increased for non-slender specimens, or reduced to around 85% of the ultimate resistance for slender specimens.

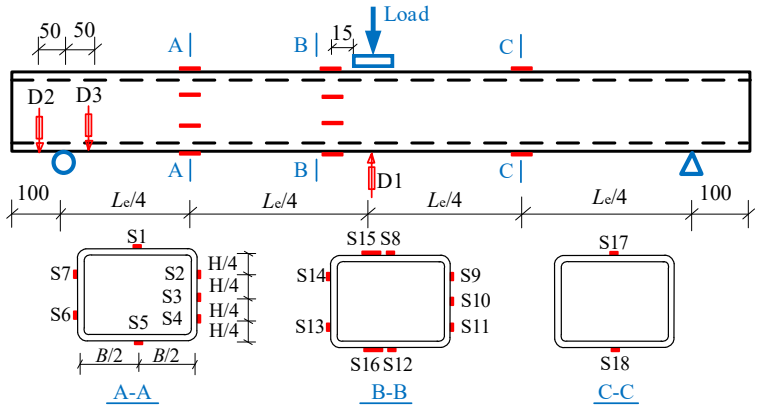

Fig. 5 Layout of LVDTs and strain gauges

3. Test results

3.1 Failure modes

The overall flexural failure with material yielding was observed for specimens with non-slender sections (i.e. class 1, 2 and 3), and meanwhile, failure modes of the brittle cracking formed at the loading point (Fig. 6 (b)), local concave deformation occurred in the compressive region (Fig. 6 (c)) were also observed. The material tensile fracture occurred suddenly for specimens STB120-B and RTB100-50-W-A, which may be due to the manufacturing imperfections of the extrusion process, as shown in Fig. 6 (a). The expected local buckling deformation was formed in the top compressive flange at the loading point for specimens RTB60-30-W-A and RTB60-30-W-B with slender sections, as illustrated in Fig. 6 (d). The failure modes of all test specimens were shown in Fig. 6(e).

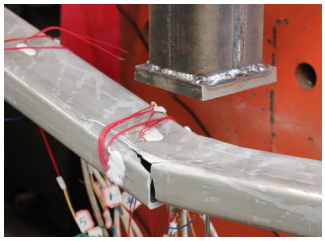

(a) Material tensile fracture (RTB100-50-W-A)

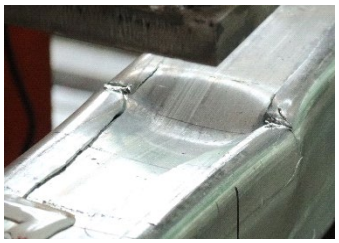

(b) Brittle cracking (STB80-A)

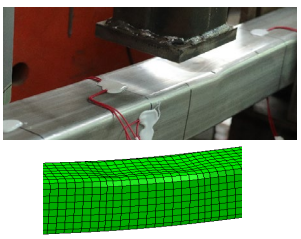

(c) Local concave deformation (STB80-B)

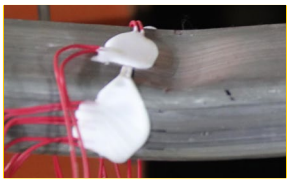

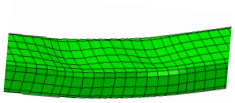

(d) Local buckling deformation (RTB60-30-W-B)

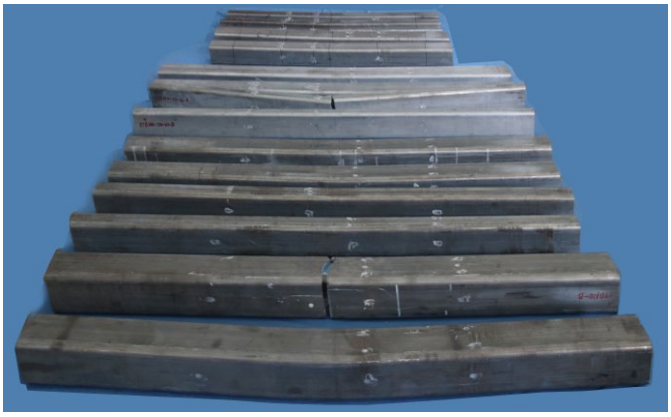

(e) All specimens after tests

Fig. 6 Failure modes of specimens

3.2 Mid-span moment-end rotation curves

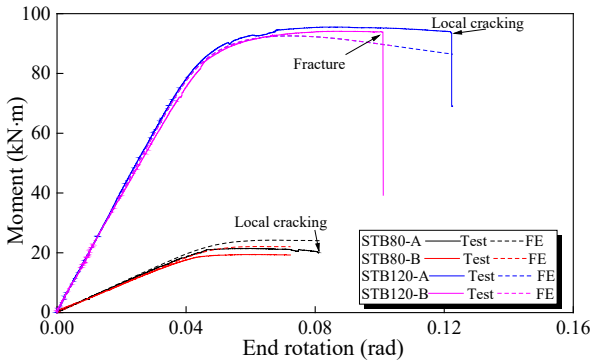

(a) STB80 and STB120

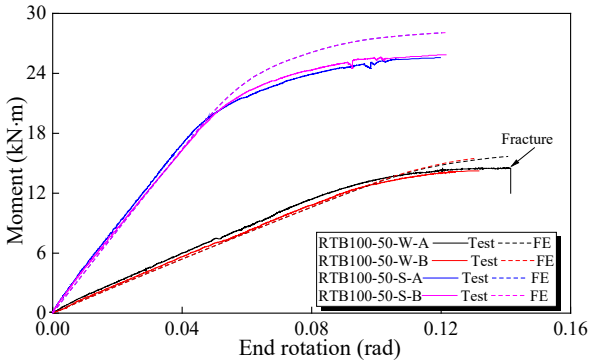

(b) RTB100-50

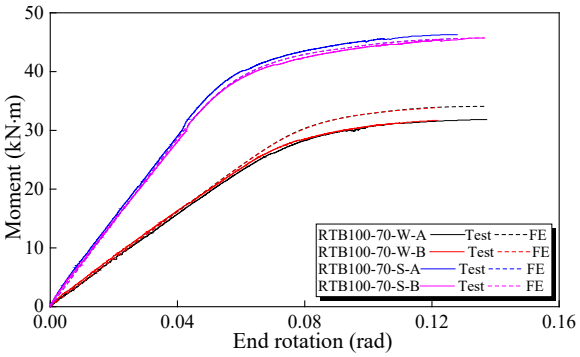

(c) RTB100-70

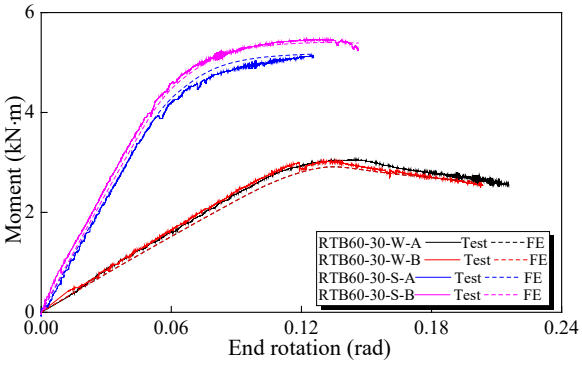

(d) RTB60-30

Fig. 7 Mid-span moment-end rotation curves

Fig. 7 shows the mid-span moment-end rotation curves of all 7A04-T6 high-strength aluminium alloy specimens subjected to three-point bending. The ultimate resistances and rotational capacities of all test specimens are summarized in Table 3, in which w_d is the ultimate mid-span deflection; $\theta_{0.2}$ and θ_u are the rotations corresponding to the yield and ultimate moment resistance, respectively; $M_{u,exp}$ and M_p are the experimental moment resistance and theoretically calculated plastic bending moment resistance,

respectively. For the specimens with non-slender sections, the mid-span moment continued to increase and their curves were almost paralleled with the horizontal axis at the final plastic stage. For the specimens with slender sections (i.e. RTB60-30-W-A and RTB60-30-W-B), a falling off in the mid-span moments appeared as the two specimens experienced local buckling deformation at the top flange. The mean ratio of $M_{u,exp}$ to M_p was 1.04, indicating that the material strain hardening has a significant effect on the cross-section capacity. Generally, all specimens had ductility defined by $\theta_u/\theta_{0.2}$ ranging from 1.76 to 3.51, and the ductility gradually decreased from class 1 to class 4 cross-sections, as stipulated in EC9-2007 [3].

Table 3 Summary of test and FE results

Specimen	w_d	$\theta_{0.2}$ (rad)	θ_u (rad)	$M_{u,exp}$ (kN·m)	M_p (kN·m)	$M_{u,FE}$ (kN·m)	θ_u /$\theta_{0.2}$	$M_{u,exp}$ /M_p	$M_{u,exp}$ /$M_{u,FE}$
STB80-A	1/25.7	0.042	0.081	21.44	23.11	24.22	1.93	0.93	0.89
STB80-B	1/30.2	0.041	0.072	19.44	21.52	22.10	1.76	0.90	0.88
STB120-A	1/19.9	0.035	0.123	95.52	86.72	61.70	3.51	1.10	1.03
STB120-B	1/24.9	0.037	0.101	94.08	88.88	61.70	2.73	1.06	1.02
RTB100-50-W-A	1/18.7	0.090	0.142	14.52	15.24	10.52	1.58	0.95	0.92
RTB100-50-W-B	1/20.1	0.096	0.132	14.23	15.42	10.50	1.38	0.92	0.90
RTB100-50-S-A	1/20.6	0.047	0.120	25.58	25.12	18.71	2.55	1.02	0.91
RTB100-50-S-B	1/21.3	0.048	0.122	25.86	25.98	18.68	2.54	1.00	0.92
RTB100-70-W-A	1/19.0	0.065	0.137	31.83	31.16	22.73	2.11	1.02	0.93
RTB100-70-W-B	1/21.0	0.064	0.122	31.69	31.05	22.63	1.91	1.02	0.93
RTB100-70-S-A	1/19.4	0.042	0.128	46.29	40.08	30.37	3.05	1.15	1.02
RTB100-70-S-B	1/18.1	0.044	0.137	45.71	41.39	30.48	3.11	1.10	1.00
RTB60-30-W-A	1/12.7	0.076	0.135	3.06	2.75	2.81	1.78	1.11	1.09
RTB60-30-W-B	1/13.9	0.075	0.131	3.04	2.75	2.81	1.75	1.11	1.08
RTB60-30-S-A	1/20.5	0.047	0.126	5.14	4.54	5.17	2.68	1.13	0.99
RTB60-30-S-B	1/16.7	0.045	0.139	5.46	4.73	5.47	3.09	1.15	1.00
Mean							2.34	1.04	0.97
COV							0.269	0.08	0.07

4. Finite element analysis

4.1 Finite element modelling

The software package ABAQUS [32] was adopted to establish finite element (FE) models for the 7A04-T6 high-strength aluminium alloy beams. The 8-node linear brick element C3D8I with incompatible modes was used to model the SHS and RHS beams, while the bearing plate at the loading

point was modelled using the element C3D8R. The true stresses (σ_{true}) and plastic strains (ε_{true}^{pl}) incorporated in FE models were calculated from measured material properties using $\sigma_{true} = \sigma(1+\varepsilon)$ and $\varepsilon_{true}^{pl} = \ln(1+\varepsilon)-\sigma_{true}/E$. The interface between the bearing plate at the loading point and the top flange of specimens was simulated by a contact pair, which was set as default hard contact and friction penalty contact with coefficient of 0.1 in the normal and tangential directions, respectively [17, 18].

The bottom flange surface with width of 100 mm at both end supports and the top surface of the bearing plate at the loading point were respectively coupled to each reference node. The two reference nodes at both end supports were free to rotate in the bending plane and translate longitudinally along specimen length, while other degrees of freedom were restrained. The reference node at the loading point were restrained against all degrees of freedom except for the translation in the vertical loading direction. The longitudinal restraint was assigned at the mid-span for all specimens. The initial local geometric imperfection amplitudes of $v_d=B/500$ [25] were integrated into FE models in accordance with the eigenvalue buckling analysis.

Table 4 Results of sensitivity analysis on specimens RTB60-30-W-A and RTB60-30-S-B

Specimen	Mesh size	$M_{u,FE}$(kN·m)	T (min)	Specimen	Mesh size	$M_{u,FE}$(kN·m)	T (min)
	2.5	2.93	47.68		2.5	5.49	44.51
	5	2.91	11.27		5	5.44	8.00
RTB	10	2.81	3.72	RTB	10	5.47	5.28
60-30-W-A	15	2.69	1.78	60-30-S-B	15	5.62	1.72
	20	2.80	1.17		20	5.58	1.37
	30	2.82	1.00		30	5.63	1.07

RTB60-30-W-A with slender section and RTB60-30-S-B with non-slender section were selected to do the mesh sensitivity analysis for the FE models. A total of 6 mesh sizes were introduced to both selected specimens. The numerical moment resistance ($M_{u,FE}$) and corresponding computational time (T) are listed in Table 4. It can be concluded that the mesh size of 10×10 mm was chosen in the present study to provide sufficient computational accuracy and take the efficiency into account simultaneously.

4.2 Validation of FE models

To evaluate the validity of the developed FE models, the comparisons between the numerical results and their experimental counterparts were made from the perspective of failure modes, moment resistance and mid-span moment-end rotation curves. As depicted in Fig. 6, some failure modes observed in the tests, including the overall bending deformation, local concave deformation and local buckling, were accurately simulated by FE models. The cracking and fracture were not observed in FE models due to the lack of tensile tests under complex stress states to calibrate the ductile fracture model. The mean value of $M_{u,exp}/M_{u,FE}$ shown in Table 3 was 0.97 with the corresponding COV of 0.07, which indicated a good agreement was achieved between the numerical and experimental results. Moreover, the mid-span moment-end rotation curves of FE models could accurately predict counterpart curves of test specimens, as shown in Fig. 7. Overall, the developed FE models herein can precisely simulate the flexural behaviour of 7A04-T6 high-strength aluminium alloy SHS and RHS beams under three-point bending.

4.3 Parametric studies

On the basis of the validated FE models, an extensive parametric study was performed to investigate the bending behaviour of the 7A04-T6 high-strength aluminium alloy SHS and RHS beams. A total of 850 FE models were developed in the present study, where the width-to-thickness ratios (b_f/t) for the beam flange in uniform compression ranged from 4 to 70 and the height-to-thickness ratios ($0.4h_w/t$) for the beam web in gradient stress varied from 0.67 to 28.33. The width or height of the cross-section of SHS and RHS varied from 36 mm to 432 mm with the width-to-height ratios being 0.23 to 3.79 for beams under weak and strong axes. Since the effective length of specimens under three-point bending showed some influence on the beam moment resistance, various aspect ratios (i.e. $(L_e\text{-}w_b)/(2H)$, in which w_b denotes the width of the bearing plate at the mid-span loading point) of 2.5, 5, 10, 15, 20, 25, 30, 35 and 40 were designed for four SHS specimens, corresponding to four classes of cross-sections,

to obtain an appropriate effective length, as shown in Fig. 8. The aspect ratio of 15 was adopted in the parametric models under the consideration of computational time and reliability of numerical results. The mean values of the measured material properties of E=73.75 GPa, $f_{0.2}$=535 MPa, f_u=607 MPa, ε_u=0.094 and n=30.3 were incorporated in all FE models. The numerical moment resistances, together with experimental results, were employed to assess the accuracy and reliability of the current design standards as well as the proposed continuous strength method (CSM) feasible for the 7A04-T6 high-strength aluminium alloy in the following sections.

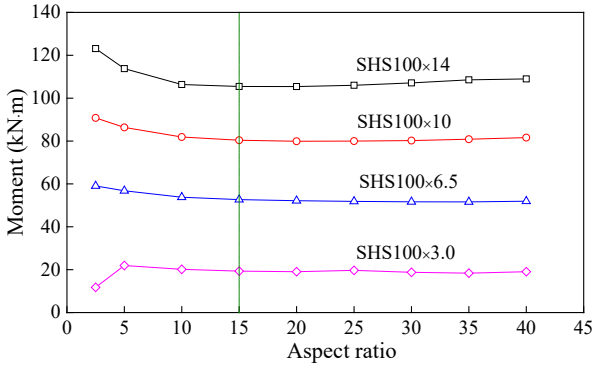

Fig. 8 Numerical results with different aspect ratios

5. Comparison between test/FE results with design standards and proposed CSM

The commonly used design methods for aluminium alloy beams in the Chinese standard GB 50429-2007 [2], the European code EC9-2007 [3] and the American design manual AA-2015 [4] were assessed for predicting moment resistance of the 7A04-T6 high-strength aluminium alloy beams. Moreover, the continuous strength method (CSM) was thoroughly modified and evaluated by the test/FE results. It should be mentioned that the resistance factors for the three design codes were all set as unity in the calculation of the moment resistances of specimens.

5.1 Chinese standard GB 50429-2007

In the current Chinese standard GB 50429-2007 [2], the effective thickness method is used to calculate the bearing capacity of aluminium alloy members with slender sections. The design moment resistance of beams is given by Eq. (1)

$$M_{\mathrm{u,GB}}=\begin{cases}\gamma_x W_{\mathrm{el}} f_{\mathrm{d}} & b/t \le 21.5\varepsilon_{\mathrm{GB}}\sqrt{k'} \\ \gamma_x W_{\mathrm{eff}} f_{\mathrm{d}} & b/t > 21.5\varepsilon_{\mathrm{GB}}\sqrt{k'}\end{cases}, \quad \text{and} \quad \frac{t_{\mathrm{e}}}{t}=\frac{1}{\bar{\lambda}}-\frac{0.22}{\bar{\lambda}^2}\le 1 \tag{1}$$

where b/t is the plate with-to-thickness ratio and expressed as b_{f}/t or h_{w}/t; W_{el} and W_{eff} are the elastic and effective section modulus, respectively; $\varepsilon_{\mathrm{GB}}$ is equal to $\sqrt{240/f_{0.2}}$; γ_x is the plastic development coefficient and taken as 1.0; f_{d} is the material design strength; k' is determined as $k/4$ for SHS and RHS beams, and k is respectively equal to $8.2/(\varphi+1.05)$ under $0<\varphi<1$, $7.81-6.29\varphi+9.78\varphi^2$ under $-1\le\varphi\le 0$ and $5.98(1-\varphi)^2$ under $\varphi<1$; φ is the stress gradient coefficient and expressed as $\sigma_{\min}/\sigma_{\max}$, in which $\sigma_{\min}$ and $\sigma_{\max}$ are the minimum and maximum stresses at the plate edges; v is the Poisson's ratio; t_{e} is the effective thickness of the plate; $\bar{\lambda}$ is the plate slenderness and equal to $\sqrt{f_{0.2}/\sigma'_{\mathrm{cr}}}$, in which σ'_{cr} is the plate elastic buckling stress.

5.2 European code EC9-2007

The European code EC9-2007 [3] is similar to GB 50429-2007 [2] in which the effective thickness method is employed for slender members with class 4 cross-sections. Apart from that, various enhancement coefficients are introduced for non-slender members to consider different levels of plastic development in cross-sections, especially for class 1 cross-sections with strain hardening effect being taken into account, as recommended in Annex F of EC9-2007 and given by Eq. (2)

$$M_{\mathrm{u,EC9}}=\begin{cases}\alpha_5 W_{\mathrm{el}} f_{\mathrm{d}} & \beta\le\beta_1 \quad \text{class 1} \\ W_{\mathrm{pl}} f_{\mathrm{d}} & \beta_1<\beta\le\beta_2 \quad \text{class 2} \\ W_{\mathrm{el}} f_{\mathrm{d}} & \beta_2<\beta\le\beta_3 \quad \text{class 3} \\ W_{\mathrm{eff}} f_{\mathrm{d}} & \beta_3<\beta \quad \text{class 4}\end{cases}, \quad \text{and} \quad \rho_c=\frac{C_1}{(\beta/\varepsilon_{\mathrm{EC9}})}-\frac{C_2}{(\beta/\varepsilon_{\mathrm{EC9}})^2} \tag{2}$$

where α_5 is the section shape coefficient and expressed as $5-(3.89+0.0019n)/(W_{\mathrm{pl}}/W_{\mathrm{el}})^{(0.27+0.0014n)}$; ρ_{c} is the reduced coefficient to factor down the thickness to obtain the effective section; C_1 and C_2 are respectively taken as 32 and 220 for aluminium alloys with T6 temper; $\varepsilon_{\mathrm{EC9}}$ is equal to $\sqrt{250/f_{0.2}}$; β is the plate with-to-thickness ratio and should consider the stress gradient for beams; β_1, β_2 and β_3 are the slenderness limits and given as $\beta_1/\varepsilon_{\mathrm{EC9}}$, $\beta_2/\varepsilon_{\mathrm{EC9}}$ and $\beta_3/\varepsilon_{\mathrm{EC9}}$ with respective values of 11, 16 and 22 for

aluminium alloys with T6 temper.

5.3 American design manual AA-2015

The design moment resistance of aluminium alloy SHS and RHS beams determined according to American design manual AA-2015 [4] takes the minimum value of the available resistance for three failure modes-member yielding, rupture and local buckling, as given by Eq. (3)

$$M_{u,AA} = \phi \min(W_{pl}F_{cy}, 1.5S_tF_{ty}, 1.5S_cF_{cy}, W_{pl}F_{tu}/k_t, F_cI_f/c_{cf}+F_bI_w/c_{cw}) \quad (3)$$

where ϕ is the resistance factor; F_{cy} and F_{ty} are the compressive and tensile yield strength, respectively; S_t and S_c are the section modulus on the tensile and compression sides of the neutral axis, respectively; F_{tu} is the tensile ultimate strength and k_t is the tension coefficient; I_f and I_w are the moments of inertia of the beam flanges and webs about the cross-section's neutral axis, respectively; c_{cf} and c_{cw} are the distances from the centreline of the beam flanges and the beam webs' extreme compression fibre to the cross-section's neutral axis, respectively; the stress F_c and F_b can be referred to B5.4.2 and B.5.5.1 of AA-2015 [4], respectively.

5.4 The continuous strength method (CSM)

The continuous strength method (CSM) [19, 33-35] is a deformation-based design approach that allows the attainment of moment resistances greater than the elastic moment capacity for non-linear materials, leading to a better prediction of structural behaviour of members with non-slender sections. The CSM has been successfully verified for providing an accurate bearing capacity of the structural stainless steel [34], carbon steel [35] and aluminium alloy [19, 33] members under bending or axial compression. However, the research to date on the CSM relevant to aluminium alloys mainly focused on the 6xxx-series aluminium alloys, which significantly differs from the 7A04-T6 high-strength aluminium alloy characterized with greater yield strength, higher ultimate strain and relatively weaker strain hardening. In view of this, the CSM extended to the 7A04-T6 high-strength aluminium alloy beams

with non-slender and slender sections was developed and discussed in the following sections.

5.4.1 Ultimate strain prediction

A total of 27 full-range stress-strain curves of the 7A04-T6 high-strength aluminium alloy from tensile coupon test results available in literatures [10, 11] and this paper were collected to determine the ultimate strain (ε_u) and strain hardening modulus (E_{sh}). The predictive expression for the ultimate strain (ε_u) was calibrated by linear regression, and given as Eq. (4)

$$\varepsilon_u = 0.356(1-f_{0.2}/f_u)+0.05 \quad (4)$$

The test ultimate strains were plotted against their predicted ones using Eq. (4), as shown in Fig. 9, together with a constant strain value being 0.08 for $f_{0.2}$>400MPa from EC9-2007 [3] and ε_u = $0.13(1-f_{0.2}/f_u)+0.059$ proposed by Su et al [19] for $f_{0.2}\leq$400MPa. It can be seen that a relatively good agreement between the test and predicted data by the proposed formula was achieved, with the mean ratio of test to predicted data being 1.0 and the corresponding COV being 0.13. While the mean values of comparison results using EC9-2007 [3] and Su et al [19] were respectively 1.09 and 1.20, and their corresponding COVs were respectively 0.16 and 0.14.

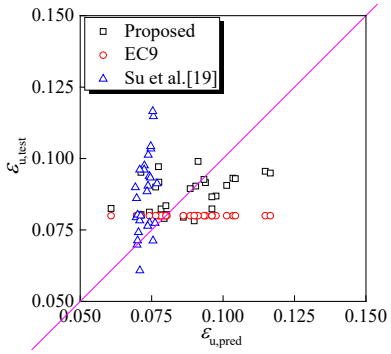

Fig. 9 Test and predicted ultimate strain

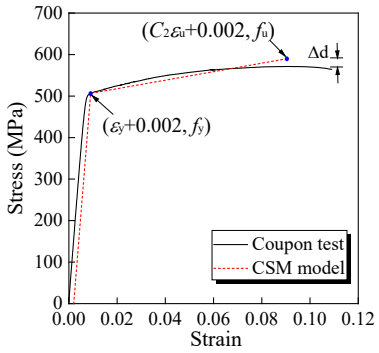

Fig. 10 Measured stress-strain curve and bi-linear model

5.4.2 Strain hardening modulus prediction

A bi-linear model simplified from the real rounded stress-strain curve is employed in the CSM to determine the strain hardening level of structural members that may be experienced [33]. The bi-linear model is composed of the elastic part and the linear hardening part with a strain hardening modulus

(E_{sh}), as illustrated in Fig. 10. Note that the linear hardening part passed through two points of (ε_y+0.002, f_y) and ($C_2\varepsilon_u$+0.002, f_u), in which ε_y=$f_{0.2}$/E; C_2 is a proportion of the ultimate strain and was calibrated based on the 27 measured stress-strain curves. The value of C_2=0.77 in Eq. (5) was found to accurately fit the measured stress-strain curves and enable the over-prediction in stress (Δ_d) to be within 5%.

$$E_{sh} = (f_u\text{-}f_{0.2})/(0.77\varepsilon_u\text{-}\varepsilon_y) \quad (5)$$

5.4.3 Base curve

The CSM base curve can be expressed by a continuous relationship between the attainable limiting strain (ε_{CSM}) divided by the yield strain (ε_y) and the cross-section slenderness ($\bar{\lambda}_p$), where $\bar{\lambda}_p$ is expressed as $\sqrt{f_{0.2}/\sigma_{cr}}$ and the elastic buckling stress σ_{cr} is recommended to be determined under the consideration of the plate interaction effect, such as the use of CUFSM programme [36]. For SHS and RHS members with non-slender sections failing after reaching the yielding moment under bending, the strain ratio $\varepsilon_{CSM}/\varepsilon_y$ is defined as (ε_y-0.002)/ε_y = ($\kappa_u y_b$-0.002)/$\kappa_e y_b$ on the basis of the plane section assumption, where κ_u and κ_{el} are the curvatures at ultimate and yielding moments, respectively; y_b is the distance from the neutral axis. For SHS and RHS members with slender sections failing before reaching the yielding moment under bending, the strain ratio $\varepsilon_{CSM}/\varepsilon_y$ is computed by M_u/M_{el}, where the M_u is the ultimate moment resistance, M_{el} is the yielding moment and equals to $W_{el}f_{0.2}$.

The CSM was extended for designing the SHS and RHS members with non-slender and slender sections under three-point bending using the test/FE results described in Sections 4 and 5. Note that the ε_{CSM} for non-slender sections was directly obtained from FE models at the moment resistance, and was conservatively determined as the ultimate strain minus by 0.002 if the moment still continues to increase slowly for stocky sections after the ultimate strain [17]. The ratio of $M_{u,exp/FE}/M_{el}$ against the cross-section slenderness ($\bar{\lambda}_p$) of the test and FE data is plotted in Fig. 11. It can be seen that the

threshold value classifying non-slender and slender sections was reasonably determined as $\bar{\lambda}_p$ =0.95 for the 7A04-T6 high-strength aluminium alloy.

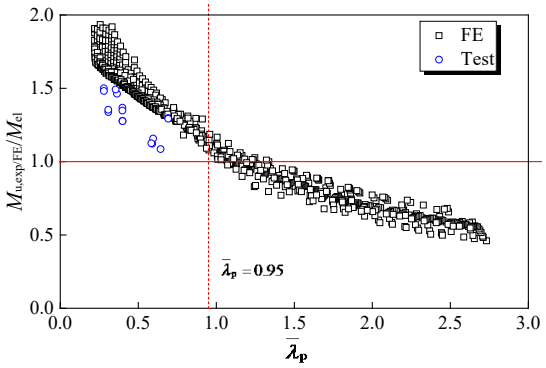

Fig. 11 Comparison of bending moment resistance with elastic moment of beams

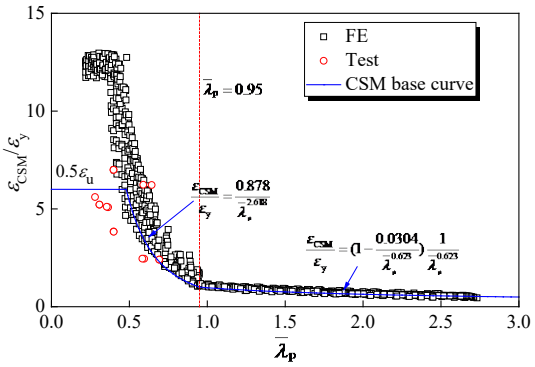

Fig. 12 Base curve for SHS and RHS with test and numerical data

The CSM limiting strain (ε_{CSM}) normalized by the yield strain (ε_y) against the cross-section slenderness ($\bar{\lambda}_p$) collected from the test and FE data is illustrated in Fig. 12, together with the fitted base curve given by Eq. (6).

$$\frac{\varepsilon_{CSM}}{\varepsilon_y}=\begin{cases}\dfrac{0.878}{\bar{\lambda}_p^{2.618}} \text{ but } \dfrac{\varepsilon_{CSM}}{\varepsilon_y}\le \text{lesser}\left(15,\dfrac{0.5\varepsilon_u}{\varepsilon_y}\right) & 0.22\le\bar{\lambda}_p<0.95\\ \left(1-\dfrac{0.0304}{\bar{\lambda}_p^{0.623}}\right)\dfrac{1}{\bar{\lambda}_p^{0.623}} & 0.95\le\bar{\lambda}_p\le 2.73\end{cases} \tag{6}$$

The form of Eq. (6) was identical to that of the 6xxx-series aluminium alloys [19]. Note that two upper limit values, being 15ε_y and 0.5ε_u for 7A04-T6 high-strength aluminium alloy beams, were taken into account for non-slender sections. The former is to limit material plastic deformation while the latter is for preventing over-prediction of material strength and material fracture.

The moment resistance of the 7A04-T6 high-strength aluminium alloy SHS and RHS members with non-slender and slender sections under three-point bending can be calculated from Eq. (7) [19].

$$M_{CSM}=\begin{cases}W_{pl}f_y\left[1+\dfrac{E_{sh}W_{el}}{EW_{pl}}\left(\dfrac{\varepsilon_{CSM}}{\varepsilon_y}-1\right)-\left(1-\dfrac{W_{el}}{W_{pl}}\right)\Big/\left(\dfrac{\varepsilon_{CSM}}{\varepsilon_y}\right)^2\right] & 0.22\le\bar{\lambda}_p<0.95\\ \dfrac{\varepsilon_{CSM}}{\varepsilon_y}M_{el} & 0.95\le\bar{\lambda}_p\le 2.73\end{cases} \tag{7}$$

5.5 Assessment of design methods

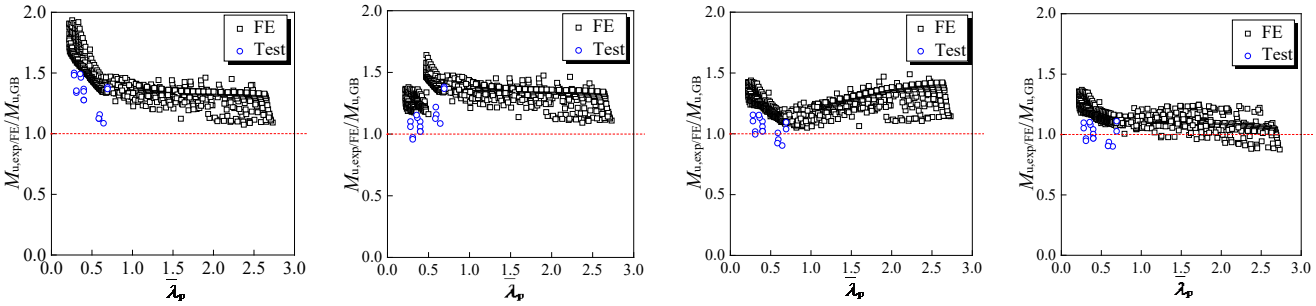

(a) Chinese standard (b) European standard (c) American standard (d) Proposed CSM

Fig. 13 Comparison of test and FE results with predicted moment resistances

Table 5 Summary of comparisons between experimental and numerical results and design strengths

Comparison	$M_{u,exp/FE}/M_{u,GB}$	$M_{u,exp/FE}/M_{u,EC9}$	$M_{u,exp/FE}/M_{u,AA}$	$M_{u,exp/FE}/M_{u,CSM}$
Mean	1.43	1.33	1.24	1.13
COV	0.117	0.072	0.077	0.074

In order to evaluate the applicability of the three current design standards and the proposed CSM for the moment resistance of the 7A04-T6 high-strength aluminium alloy SHS and RHS members, a total of 866 test/FE results were compared with those from the four design methods, as plotted in Fig. 13. The quantitative mean values and corresponding COVs of the moment ratios are listed in Table 5. The GB 50429-2007 provided the most conservative and scattered predictions, with the mean value of $M_{u,exp/FE}/M_{u,GB}$ and corresponding COV being 1.43 and 0.117, respectively, due to lack of consideration on the section plastic development. The calculated results from EC9-2007 were improved by 10% compared with those from GB 5042-2007, which is resulted from the more accurate design approach in Annex F. A less conservative and more scattered results determined according to AA-2015 ($M_{u,exp/FE}/M_{u,AA}$=1.24 and COV=0.077) was observed. The reason is that AA-2015 can better predict the moment resistance of members with $\bar{\lambda}_p$ being around in the range of 0.5~1.1. The predicted moments from the proposed CSM were found to be much more accurate and less scattered than those from GB 50429-2007, EC9-2007 and AA-2015, with mean value of $M_{u,exp/FE}/M_{u,CSM}$ and corresponding COV being 1.13 and 0.074, respectively, indicating the moment resistance of 7A04-T6 high-strength aluminium alloy SHS and RHS members under three-point bending can be well predicted by the proposed CSM.

6. Reliability analysis

6.1 Resistance and load variables

The material strength, geometric properties and the model error are the three key random variables of the beam resistance and their uncertainties would impose a great influence on the reliability analysis results. According to the coupon and specimen tests in References [10, 11] and this paper, the statistical parameters of the mean value of $f_{0.2}$ and corresponding COV for the 7A04-T6 high-strength aluminium alloy were respectively determined as 534.47 MPa and 0.043, and those values of geometric dimensions were respectively set as 1.003 and 0.013. The model error is defined as the ratio of the test or FE results to the predicted moment resistance as shown in Table 5. Note that these three random variables about the beam resistance were all assumed to be normally distributed.

Table 6 Load combinations of different design standards

Combination	GB 50068-2018 [39]	EN1990 [40]	ASCE7-2010 [41]
S_{DL}+S_{RLL}	1.3S_{DL}+1.5S_{RLL}	1.35S_{DL}+1.5S_{RLL}	1.2S_{DL}+1.6S_{RLL}
S_{DL}+S_{OLL}	1.3S_{DL}+1.5S_{OLL}	1.35S_{DL}+1.5S_{OLL}	1.2S_{DL}+1.6S_{OLL}
S_{DL}+S_{WL}	1.3S_{DL}+1.5S_{WL}	1.35S_{DL}+1.5S_{WL}	0.9S_{DL}+1.0S_{WL}
S_{DL}+S_{RLL}+S_{WL}	1.3S_{DL}+1.5S_{RLL}+0.9S_{WL}	1.35S_{DL}+1.5S_{RLL}+0.9S_{WL}	1.2S_{DL}+1.0S_{RLL}+1.6S_{WL}
S_{DL}+S_{RLL}+S_{WL} +S_{SL}	1.3S_{DL}+1.5S_{RLL} +0.9S_{WL}+1.05S_{SL}	1.35S_{DL}+1.5S_{RLL} +0.9S_{WL}+1.05S_{SL}	1.2S_{DL}+1.0S_{RLL} +1.0S_{WL}+0.5S_{SL}

A total of 5 types of loads, including the dead load (S_{DL}), residential live load (S_{RLL}), office live load (S_{OLL}), wind load (S_{WL}) and snow load (S_{SL}), were considered to form various load combinations that may be encountered by structures. The statistical parameters of the five loads in terms of the distribution type, ratio of nominal to mean values and COVs are specified in References [2, 37, 38] corresponding to Chinese, European and American codes, respectively. Five forms of load combination with different partial factors according to three standards were used to calculate reliability indices, as summarized in Table 6. Additionally, the load ratios of $\rho = S_{RLL}/S_{DL}$, S_{OLL}/S_{DL}, S_{WL}/S_{DL} or S_{SL}/S_{DL} and $\alpha = S_{WL}/S_{RLL}$ or S_{SL}/S_{RLL} were introduced herein to assess the influence of the load ratio on the reliability, which were respectively taken as (0.1, 0.25, 0.5, 1, 2, 3, 4) and (0.25, 0.5, 1, 2, 4). Note that

the statistical parameters of loads, load combinations and resistance factors of the proposed CSM are the same as those of GB 50429-2007 under the assumption that the beam specimens made of 7A04-T6 high-strength aluminium alloy are extruded and applied in China.

Since no resistance factor (ϕ) and design strength (f_d) of the 7A04-T6 high-strength aluminium alloy are stipulated in the three current standards, the resistance factors ϕ=1/1.2=0.833, ϕ=1/1.1=0.91 and ϕ=0.90 for the 6xxx-series ordinary aluminium alloys in GB 50429-2007, EC9-2007 and AA-2015 were applied herein. According to the 27 collected tensile coupon test data, the statistical design yield strengths were respectively obtained as 410 MPa and 450 MPa, and the design ultimate strengths were respectively determined as 460 MPa and 500 MPa for GB 50429-2007 and EC9-2007. The statistical nominal yield and ultimate strengths were respectively taken as 495 MPa and 550 MPa for AA-2015.

6.2 Analysis results

The relationship between the reliability index (β) and the load ratio (ρ) for the four design approaches is plotted in Fig. 14, where β is the mean value of indices for all the five load combinations under the same ρ. The recommended target reliability index specified in GB 50429-2007, EC9-2007 and AA-2015 for aluminium alloy beams are β_{GB}=3.7, β_{EC9}=3.8, and β_{AA}=2.5, respectively, which are also presented in Fig. 14. As observed, the reliability indices of EC9-2007 were the highest among the four design methods, while GB 50429-2007 and the proposed CSM took the second and third places. The AA-2015 showed the lowest reliability level. All the calculated reliability indices of the four design methods exceeded respective target values, which demonstrated that the four design methods were robust and safe for the high-strength aluminium alloy beam members. It may be concluded that the proposed CSM can provide accurate and reliable design resistance for the 7A04-T6 high-strength aluminium alloy SHS and RHS beam members under moment gradient.

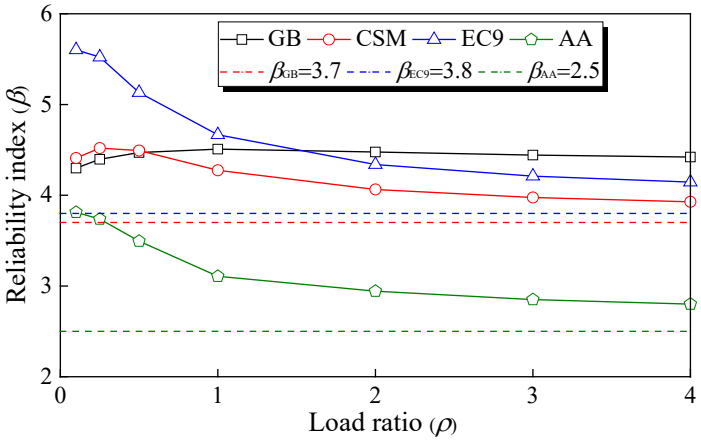

Fig.14 Reliability index of the four design methods

7. Conclusions

An experimental and numerical investigation on the flexural behaviour of extruded 7A04-T6 high-strength aluminium alloy SHS and RHS beams subjected to a moment gradient loading has been presented in this paper. The main conclusions drawn are as follows:

(1) The failure modes of the overall flexural failure with material yielding, local concave deformation, brittle cracking and material tensile fracture were observed for specimens with non-slender sections, while local buckling deformation formed in the compressive flanges for specimens with slender sections.

(2) The mid-span moments of specimens with non-slender sections tended to be constants at late loading stage because of strain hardening effect of aluminium alloys, while a falling off in the mid-span moments of specimens with slender sections appeared as local buckling occurred.

(3) The current design standards of GB 50429-2007, EC9-2007 and AA-2015 were relatively conservative in predicting the moment resistance of 7A04-T6 high-strength aluminium alloy SHS and RHS beams, especially for GB 50429-2007 with under-estimation up to 43% due to ignorance of the plastic development of non-slender sections. The proposed CSM herein extended to the 7A04-T6 high-strength aluminium alloy SHS and RHS beams under moment gradient was found to offer the most accurate and less scattered predictions.

(4) The reliability level obtained from EC9-2007 was the highest, followed by GB 50429-2007 and the proposed CSM, and AA-2015 provided the lowest reliability. All the reliability indices exceeded corresponding target reliability limits, indicating the four design methods were safely applicable to design the high-strength aluminium alloy beams.

Acknowledgements

The authors would like to acknowledge the financial supports provided by the National Natural Science Foundation of China (Grants NO. 52108154 and No.51878377), the China National Postdoctoral Program for Innovative Talents (Grant No. BX20200193) and the China Postdoctoral Science Foundation (Grant No. 2021M691826).

References

[1] Georgantzia E, Gkantou M, Kamaris G. Aluminium alloys as structural material: A review of research. Engineering Structures, 2021, 227:111372.

[2] GB 50429-2007. Code for design of aluminium structures. Beijing: China Planning Press, 2007 (in Chinese).

[3] Eurocode 9 (EC9): Design of aluminium structures. Part 1-1: General structural rules-General structural rules and rules for buildings. BS EN 1999-1-1:2007, European Committee for Standarization (CEN):2007.

[4] Aluminum Association (AA). Aluminum design manual. Washington DC, 2015.

[5] Zhang Y, Wang YQ, Li BB, Wang ZX, Liu XC, Zhang JG, Ouyang YW. Structural behaviour of the aluminium alloy Temcor joints and Box-I section hybrid gusset joints under combined bending and shear. Engineering Structures, 2021, 249: 113380.

[6] Zhang DN, Shangguan QQ, Xie CJ, Liu F. A modified Johnson-Cook model of dynamic tensile behaviours for 7075-T6 aluminum alloy. Journal of Alloys and Compounds, 2015, 619:186-194.

[7] Wang YQ, Wang ZX. Experimental investigation and FE analysis on constitutive relationship of high strength aluminum alloy under cyclic loading. Advances in Materials Science and Engineering, 2016, 2016:1-16.

[8] Chen ZH, Lu J, Liu HB, Liao XW. Experimental investigation on the post-fire mechanical properties of structural aluminum alloys 6061-T6 and 7075-T73. Thin-Walled Structures, 2016, 106:187-200.

[9] Karolczuk A, Kluger K, Palin-Lu T. Fatigue failure probability estimation of the 7075-T651 aluminum alloy under multiaxial loading based on the life-dependent material parameters concept. International Journal of Fatigue, 2021, 147:106174.

[10] Wang YQ, Wang ZX, Hu XG, Han JK, Xing HJ. Experimental study and parametric analysis on the stability behaviour of 7A04 high-strength aluminum alloy angle columns under axial compression. Thin-Walled Structures, 2016, 108:305-320.

[11] Wang ZX, Wang YQ, Yun X, Gardner L, Hu XG. Experimental and numerical study of fixed-ended high-strength aluminum alloy angle-section columns. Journal of Structural Engineering, 2020, 146(10): 04020206.

[12] Rong B, Guo Y, Li ZY. Study on the stability behavior of 7A04-T6 aluminum alloy square and rectangular hollow section columns under axial compression. Journal of Building Engineering, 2022, 45: 103652.

[13] Moen LA, Hopperstad OS, Langseth M. Rotational capacity of aluminum beams under moment gradient. I: Experiments. Journal of Structural Engineering, 1999, 125(8):910-920.

[14] Zhu JH, Young B. Design of aluminum alloy flexural members using direct strength method. Journal of Structural Engineering, 2009, 135(5):558-66.

[15] Kim Y, Peköz T. Ultimate flexural strength of aluminum sections. Thin-Walled Structures, 2010, 48:857-865.

[16] Su MN, Young B, Gardner L. Deformation-based design of aluminium alloy beams. Engineering Structures, 2014, 80:339-349.

[17] Su MN, Young B, Gardner L. Continuous beams of aluminum alloy tubular cross sections. I: Tests and FE Model Validation. Journal of Structural Engineering, 2015, 141(9):04014232.

[18] Su MN, Young B, Gardner L. Flexural response of aluminium alloy SHS and RHS with internal stiffeners. Engineering Structures, 2016, 121:170-180.

[19] Su MN, Young B, Gardner L. The continuous strength method for the design of aluminium alloy structural elements. Engineering Structures, 2016, 122:338-348.

[20] Feng R, Sun W, Shen CD, Zhu JH. Experimental investigation of aluminum square and rectangular beams with circular perforations. Engineering Structures, 2017, 151:613-32.

[21] Feng R, Chen ZM, Shen CD, Roy K, Chen BS, Lim JBP. Flexural capacity of perforated aluminium CHS tubes-An experimental study. Structures, 2020, 25:463-480.

[22] Castaldo P, Nastri E, Piluso V. Ultimate behaviour of RHS temper T6 aluminium alloy beams subjected to non-uniform bending: Parametric analysis. Thin-Walled Structures, 2017, 115:129-141.

[23] Castaldo P, Nastri E, Piluso V. FEM simulations and rotation capacity evaluation for RHS temper T4 aluminium alloy beams. Composites Part B, 2017, 115: 124-137.

[24] Piluso V, Pisapia A, Nastri E, Montuori R. Ultimate resistance and rotation capacity of low yielding high hardening aluminium alloy beams under non-uniform bending. Thin-Walled Structures, 2019, 135:123-136.

[25] Nastri E, Piluso V. The influence of strain-hardening on the ultimate behaviour of aluminium RHS-beams under moment gradient. Thin-Walled Structures, 2020, 157:107091.

[26] Nastri E, Piluso V, Pisapia A. Numerical application of effective thickness approach to box aluminium sections. Journal of Composite Science, 2021, 5, 291.

[27] Zhao YZ, Zhai XM. Bending strength and design methods of the 6082-T6 aluminum alloy beams with circular hollow sections. Structures, 2020, 26(2):870-887.

[28] Bock M, Theofanous M, Dirar S, Lipitkas N. Aluminium SHS and RHS subjected to biaxial bending: Experimental testing, modelling and design recommendations. Engineering Structures, 2021, 227: 111468.

[29] Zhang Y, Wang YQ, Wang ZX, Bu YD, Fan SG, Zheng BF. Experimental investigation and numerical

analysis of pin-ended extruded aluminium alloy unequal angle columns. Engineering Structures, 2020, 215: 110694.

[30] GB/T 228.1-2010. Metallic materials-Tensile testing-Part 1: Method of test at room temperature. Beijing: China Standards Press, 2008. (in Chinese)

[31] Ramberg W, Osgood WR. Description of stress strain curves by three parameters: technical note 902. Washington DC: National Advisory Committee for Aeronautics, 1943, 1-12.

[32] Dassault Systemes. ABAQUS/Standard user's manual volumes I-III and ABAQUS CAE manual - Version 6.19. UK: Simulia Corporation; 2014.

[33] Su MN, Young B, Gardner L. Testing and design of aluminium alloy cross-sections in compression. Journal of Structural Engineering, 2014, 140(9): 04014047.

[34] Afshan S, Gardner L. The continuous strength method for structural stainless steel design. Thin-Walled Structures, 2013, 68:42-49.

[35] Lan XY, Chen JB, Chan TM, Young B. The continuous strength method for the design of high strength steel tubular sections in bending. Journal of Constructional Steel Research, 2019, 160:499-509.

[36] Li Z, Schafer BW. Buckling analysis of cold-formed steel members with general boundary conditions using CUFSM: conventional and constrained finite strip methods, Missouri University of Science and Technology, Rolla, MO, USA, 2010.

[37] SAKO. Joint Committee of NKB and INSTA-B. Design basis of structures. Proposal for modification of partial safety factors in Eurocodes. 1999.

[38] Maria MS, Andrzej SN. Calibration of design code for buildings (ACI 318): Part 2-Reliability analysis and resistance factors. ACI Structural Journal, 2003, 100: 383-391.

[39] GB 50068-2018. Unified standard for reliability design of building structures. Beijing: China Construction Industry Press, 2018 (in Chinese).

[40] EN 1990-Eurocode: Basis of structural design. European Committee for Standardization, Brussels, 2001. American Society of Civil Engineers, Reston, 2010.

[41] ASCE 7-10. Minimum design load for buildings and other structures. American Society of Civil Engineers, Reston, 2010.